Geophys. J. Int. (2002) **151,** 612–621

Time-dependent effects in elastoviscoplastic models of loaded lithosphere

Richard A. Albert* and Roger J. Phillips

McDonnell Center for the Space Sciences and Department of Earth and Planetary Sciences, Washington University, St. Louis, MO 63130 *USA.*
E-mails: albert@es.usyd.edu.au; phillips@wustite.wustl.edu

Accepted 2002 June 25. Received 2002 June 20; in original form 2001 October 11

SUMMARY

We conducted a plane strain finite element analysis of topographic loading on a 40-km-thick, compositionally homogeneous, wet olivine oceanic lithosphere. The rheological model was elastoviscoplastic (EVP) and accommodated elastic deformation, steady-state dislocation creep, as well as frictional slip via a Drucker–Prager yield surface. From the model results, we analyse the development of thrust and normal faulting zones that evolve with the growth of a 150 MPa spatially uniform topographic load, as well as the interaction between frictional slip and creep in the normal faulting zone that exists at about 20 km depth beneath the load. The spatial extent of this zone is shown to be a function of the load growth rate, and during loading, the lowest 3 km of this region demonstrates simultaneous pressure-sensitive frictional slip and pressure-insensitive, temperature- and strain rate-dependent creep. This dual-mechanism deformation is similar to descriptions of semi-brittle deformation because of the combined cataclastic and crystal-plastic nature that characterizes semi-brittle flow. The models also show a feature that we refer to as palaeoslip. Within the two normal faulting regions in the lithosphere (and after the load has reached its maximum), part of each region maintains active faulting while nearby the faulting has long since ceased. The active faulting is enabled by the migration of stress due to post-loading creep in high temperature regions of the plate. These three phenomena cannot be realized in elastic-plastic or viscoelastic rheologies.

Key words: creep, finite element analysis, flexure of the lithosphere, lithosphere, lithosphere deformation, rheology.

1 INTRODUCTION

The combination of rock mechanics laboratory experiments with numerical analysis provides the best approach to understanding the Earth's lithospheric response to loading. One of the widely used techniques that combines these approaches is the Yield Strength Envelope (YSE) formulation (Goetze & Evans 1979; Brace & Kohlstedt 1980; Kirby 1983). The YSE has been used in conjunction with an elastic–perfectly plastic (EP) formulation to model the allowable lithospheric deformation at regions on Earth (Watts *et al.* 1980; Bodine *et al.* 1981; McNutt & Menard 1982; Karner *et al.* 1993; Burov & Diament 1995, 1996; Cloetingh & Burov 1996; Kohlstedt *et al.* 1995; Mueller & Phillips 1995), as well as Venus (Phillips 1990; Brown & Grimm 1996), and Mars (Solomon & Head 1990) by incorporating Byerlee's rule for frictional slip of rocks (Byerlee 1978) with an empirically determined steady-state (secondary) creep law (Carter 1976; Poirier 1985; Carter & Tsenn 1987) for the rock type(s) adopted. With these material relationships, a brittle mechanism and crystal-plastic (macroscopically continuous, ductile) (Rutter 1986; Paterson 1978) aspect of lithospheric deformation are represented. We note that it is an oversimplification to indicate that earthquakes will occur at depths where Byerlee's rule is satisfied in YSE/EP analyses. The formulation does not address the stability versus instability of slip that governs seismicity on faults (Tse & Rice 1986; Scholz 1998), as we will discuss in Section 2.

Despite the success of the YSE/EP approach, it contains another major limitation, namely that, as it is most commonly employed, it provides no information on the time-dependent strength of the lithosphere in response to loading. We utilized the concept of an elastoviscoplastic (EVP) yield strength envelope (Albert *et al.* 2000) to specifically incorporate time-dependent behaviour. In that paper, we compared results from this finite element EVP model to the EP output of an identically loaded, YSE-constrained, wet olivine lithosphere with identical material parameters and loading. We focused on the deviations in the ductile creep zones from the isostrain rate contours of the YSE/EP analysis; in the pressure-sensitive, frictional slip areas we noted the load's effect on the mean stress for rock lying beneath the load. This resulted in larger plate bending

*Now at: Division of Geology & Geophysics, Edgeworth David Bldg F05, University of Sydney, Sydney, NSW 2006, Australia.

moments under the load relative to analyses that ignore the load's role in strengthening underlying rock.

In this paper we cover three additional topics that were not included in Albert *et al.* (2000). The first aspect is the dependence of the spatial distribution of faulting in the lithosphere on the load growth rate. EVP models show interplay between the load growth rate, the viscous relaxation of stress at high temperatures, and the occurrence of frictional slip at suitable differential stresses. The second focal point of this paper is the appearance of 'palaeoslip' at the frictional slip to creep transition and elsewhere. Palaeoslip is our description of areas of prior frictional slip that cease faulting after the load stops growing, while nearby rock continues to slip. That is, our models show that at times beyond the load growth period some areas of slip have become passive while others areas remain active.

Thirdly, our models also show a narrow transitional zone between purely brittle failure (via frictional slip) and exclusively ductile deformation (via dislocation creep). In this transitional region we find simultaneous brittle frictional slip and ductile dislocation creep, that is, the pressure-temperature-strain rate conditions favor both of these mechanisms at the same time. We note the similarity between this narrow transitional zone and semi-brittle deformation; both are characterized by combined pressure-sensitive cataclastic and pressure-insensitive crystal-plastic mechanisms.

2 THE EVP RHEOLOGY

An important aspect of our rheological model is that every element in the mesh has the potential for elastic, viscous, and plastic deformation. We do not constrain a specific type of deformation to operate in a certain area, so that frictional slip, crystal-plastic, and transitional zones between the rheologies arise from the empirical constitutive relations and the conditions developed in the model. The EVP rheological model is represented by the usual spring and dashpot in series from Maxwell viscoelasticity (non-Newtonian, in this case) but additionally has a plastic 'sliding block' in series with the other two components. The plastic part of the model is not crystal-plasticity with its time-dependent, continuous, distributed deformation via dislocation slip or twinning, but is instead the time-independent, discontinuous, frictional slip on a pervasively fractured rock mass (Byerlee 1978). The model accommodates this frictional slip plasticity by employing a linear Drucker–Prager yield surface (Zienkiewicz & Taylor 1989), which can be thought of as a smooth (with the exception of the vertex at the surface's tip) conical surface centered on the hydrostatic axis in principal stress space, with the cone expanding in the direction of increasing hydrostatic pressure. The Drucker–Prager surface models the high stress branch of Byerlee's rule (defined by Byerlee as having a minimum principal stress in excess of 110 MPa) with a cohesion of 50 MPa and a base friction coefficient of 0.6 (corresponding to an internal friction angle of 30°); the shallower, low stress branch of Byerlee's rule is neglected for simplicity.

The base friction coefficient determines the frictional strength of the rock but has no impact on the frictional instability that governs seismogenesis (Rutter 1993; Scholz 1998). Therefore, our rheological model is not pertinent to predictions of seismicity, which are related to the issue of slip stability and not solely related to fault strength as given by Byerlee's rule. Models that relate the friction coefficients to the *rate* of slip, and the *state* or physical properties of the slip surfaces (so-called rate- and state-variable friction laws) are needed to determine whether a slip event will cause an earthquake (Dieterich 1979; Ruina 1983; Tse & Rice 1986). However, we can look upon areas in our models that undergo frictional slip as potentially seismic wave-inducing, and Byerlee's rule can in general be treated as a necessary but insufficient condition (in the absence of complicating factors such as stress concentrations, etc.) for the generation of earthquakes. Because the magnitude of the rate- and state- changes to the operative friction coefficients are generally small, it is unlikely that seismicity will occur if the stresses are well below that of this base level (J.W. Rudnicki, private communication, 2001).

As an additional simplification, we utilize an associated flow rule for plasticity so that the dilation factor and internal friction factors are identical (Khan & Huang 1995; Zienkiewicz & Taylor 1989) for computational simplicity. Although these parameters are not generally identical for rock, and each may vary over the course of loading (Ord *et al.* 1991; Albert & Rudnicki 2001), equating them should not significantly alter the results we present here. Related to the above point, we also neglect any effects of strain-hardening, strain-softening, and localization that are frequently pertinent to problems of lithospheric deformation involving multiple time- and length-scales (Rudnicki & Rice 1975; Poirier 1980; Read & Hegemier 1984; Kirby & Kronenberg 1987; Bažant 1988; Burg 1999).

The EVP rheology has been implemented before (Braun & Beaumont 1987, 1989; Bassi 1991; Bassi *et al.* 1993; Chéry *et al.* 1992; Beaumont *et al.* 1996; Batt & Braun 1997; Gerbault *et al.* 1999; Cloetingh *et al.* 1999; Huismans *et al.* 2001) with respect to deformation at rift zones and compression orogens and with some variations relative to our scheme. Other EVP models include investigations ductile failure via plastic shear heating (Regenauer-Lieb & Yuen 1998), and the initiation of subduction (Regenauer-Lieb *et al.* 2001).

3 METHODOLOGY

We employed four time-varying loading simulations (involving a maximum load of 150 MPa) to gain insight into how creep strain rates, stress distribution, and both elastic and inelastic strains evolve with time in a model with EVP rheology. The model was not intended to model any particular location on Earth (other than oceanic lithosphere of moderate age) but was rather a fundamental study of how such a complex rheological model for rock responds to loads of a geological magnitude on a geological timescale. We used the commercially available MARC Finite Element Software (MARC Analysis Research Corporation, version K6.2 1994). Five thousand quadrilateral plane strain elements with bilinear shape functions simulated a 40 km deep by 700 km length lithospheric plate of wet olivine (with parameters similar to those of Karato *et al.* 1986) of moderate strength. Because the simulations involved bending of a discretization composed of continuum (as opposed to structural) elements, we included MARC's assumed strain formulation to avoid shear locking (Bathe 1996) and utilized an updated Lagrangian formulation to properly account for finite strains. The initial stress distribution was lithostatic (Engelder 1993) and the temperature distribution in the plate was a linear steady-state conduction profile with a temperature of 1073 K at 40 km depth and 273 K at the top surface of the plate. The plate's Young's modulus and Poisson ratio were 1.6×10^{11} Pa and 0.28, respectively. The inclusion of gravity was crucial to providing a proper model for pressure-dependent yield via a cataclastic process. With this thickness and temperature distribution, the plate age corresponded to an oceanic lithosphere of 35 Myr (Turcotte & Schubert 1982). A more detailed discussion of the methodology for these models can be found in Albert *et al.* (2000).

The bottom of the plate at 40 km depth was the lithosphere–asthenosphere boundary and was represented by a Winkler

foundation with a normal traction (only) of $\Delta\rho g y$, where y was the deflection of the plate into the foundation, g is gravity, and the density contrast $\Delta\rho$ was 2300 kg m^{-3} (asthenosphere density minus seawater density). The left and right sides of the plate were symmetry boundaries; the uniform load extended 90 km from the right ('loading') axis and the rest of the boundary was stress free. The topographic load grew linearly from zero to a maximum of 150 MPa, during 'loadtimes' (LT) of 0 (instantaneous loading), 0.1 Myr, 1.0 Myr, and 10 Myr. For times beyond the LT for a particular simulation the load remained constant at 150 MPa as a 'dead' load. For simplicity, we used a spatially uniform load, which will overemphasize the magnitude of the deformational response relative to a tapered load. In addition, because of our use of a plane strain (as opposed to an axisymmetric) formulation, it should be noted that the amount of deformation in the plate is more extensive relative to an axisymmetric case.

The steady-state dislocation creep relation between effective strain rate, $\dot{\varepsilon}_c$, and effective shear stress, σ_d, involves an activation energy (Q) of 420 000 J mol^{-1}, a creep coefficient (A) of 600 MPa$^{-3.0}$ s^{-1}, and a stress exponent (n) of 3.0.

$$\dot{\varepsilon}_c = A \cdot \sigma_d^n \exp\left(-\frac{Q}{RT}\right) \tag{1}$$

In eq. (1), $\sigma_d = (\sigma_1 - \sigma_3) \approx (\sigma_H - \sigma_V)$, where σ_1 and σ_3 are principal stresses, and σ_H and σ_V are horizontal and vertical stresses, respectively. For the Drucker–Prager frictional slip we used the high stress branch of Byerlee's rule (Byerlee 1978). The high stress branch governed frictional slip in rocks for effective normal stresses ($\bar{\sigma}_n$) in excess of 200 MPa.

$$\tau = 0.6\bar{\sigma}_n + 60 \pm 10 \tag{2}$$

A cohesion of 50 MPa and a 30° internal friction angle were used. Note that the 30° internal friction angle corresponded to a base friction coefficient of about 0.6, as stated in Section 2.

4 RESULTS

Fig. 1 shows the plastic strains (frictional slip) in the bending direction for the $LT = 10$ Myr simulation at the final time of ≈42 Myr. Zones of plasticity are, by the continuum approach used here, regions of faulting, i.e. plastic strain implies relief of stress by faulting. Plasticity occurs at two locations along the right (loading) symmetry axis. At the top there is a zone of thrust faulting directly under the load. In the depth interval 17–27 km, there is a region of normal faulting that lies directly above the creep zone and also overlaps the creep zone over a few km. We refer to this normal faulting zone as the 'loading-axis deep slip zone' (LAD slip zone) throughout this paper. Also in this model is a shallow region of plasticity (normal faulting) at the flexural bulge between 120 km and 230 km from the loading axis. We refer to this zone as the 'lateral slip zone'.

The development of these slip zones is readily understood considering the nature of the loading. The LAD slip zone arises in conjunction with creep occurring near the bottom of the plate. Relief of stresses by viscous relaxation of in the lithosphere leads to the upward migration of tensional stresses to lower temperatures/shallower depths, in the region of frictional slip. The other two zones of plastic failure are easily understood in terms classical plate flexure and the YSE. Normal faulting in the flexural bulge has been discussed by Bodine *et al.* (1981) and Schultz & Zuber (1994), for example, but the potential seismicity is difficult to observe, requiring teleseismicity and earthquakes of sufficient magnitude ($m_b \geq 5.5$) (McGovern & Solomon 1994).

4.1 Zone of plastic failure depends on LT

Fig. 2 shows that the spatial extent of the LAD slip zone at the end of a model run ($t \approx 42$ Myr) is a strong function of the loading rate. For the instantaneous loading case ($LT = 0$) this failure region covers the greatest depth (17 km–36 km); the longest load growth period ($LT = 10$ Myr) shows the smallest region of slip (17 km–27 km). The dependence of the spatial extent of the loading-axis slip on the loading time is due to the time effects of creep. The $LT = 0$ case shows the greatest depth of slip because the load is emplaced so quickly that the time required for significant stress relaxation via creep cannot be reached before frictional slip occurs. Loads that grow more slowly allow creep to relax the more tensional bending stresses that develop where the temperatures are sufficiently high. As a result, the extent of the LAD slip zone decreases as the loading time increases. The extent of pressure-sensitive, brittle deformation via cataclastic processes at great depth should be controlled by whether this deformation mechanism can exist based on the $P - T - \dot{\varepsilon}$ conditions and the degree to which time-dependent creep can bring differential stresses below the rock strength at a given depth.

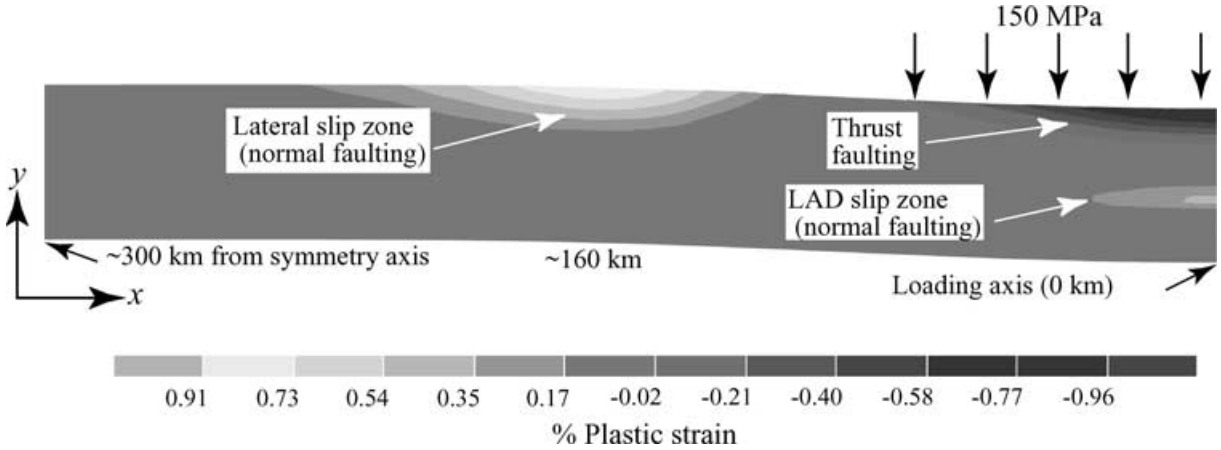

Figure 1. A plot of the plastic (frictional slip) strains in the bending direction throughout the plate at the final time of the simulation ($t \approx 42$ Myr). The model has a final load of 150 MPa growing linearly over $LT = 10$ Myr. Two zones of normal faulting and one zone of thrust faulting arise in the plate. The convention is that positive stresses and strains are extensional.

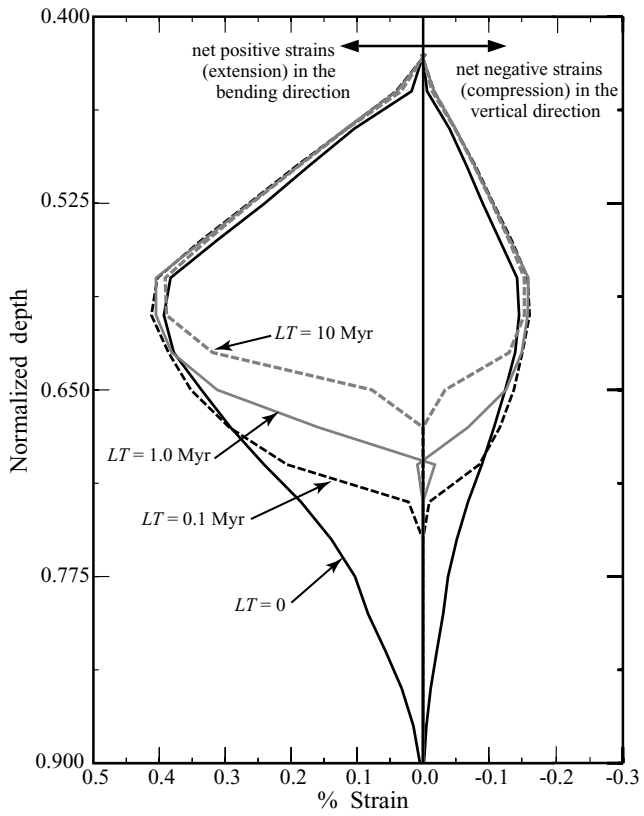

Figure 2. The extent of plastic strains in the LAD slip zone (with the depth normalized by the plate thickness) as a function of *LT* at the end of the model runs ($t \approx 42$ Myr). As *LT* is increased the growth rate is slowed and creep has the time to relax the differential stresses as they build up. This effect occurs for areas at sufficiently high temperature. The curves also show the manner in which elements in this zone are vertically compressed and laterally extended under the topographic load.

4.2 Palaeoslip

The LAD slip zone does not show active slip over its entirety after *LT*. The deepest parts of the LAD slip zone cease to slip and the stresses relax by the end of the load growth period, while the shallower parts of the zone continue faulting until the end of the simulation (≈42 Myr). This distinction leads to palaeoslip and active-slip designations, as discussed below. Note that Fig. 2 shows the cumulative effect of all slippage (total plastic strain) throughout the model history and does not provide information on the extent of active normal faulting (as would be inferred from the plastic strain rate) at the final time in the simulations.

Bending stresses, bending plastic strains, and bending creep strains in the LAD slip zone are shown in Figs 3, 4(a) and (b), respectively. Fig. 3 shows that the in-plane horizontal stress (σ_{xx}) at the initial time increases compressionally with depth, according to the lithostatic stress state ($\sigma_{xx} = \sigma_{zz} =$ lithostatic stress, σ_{yy}). Subsequently, the entire LAD slip zone shows the development of more tensional bending stresses (i.e. compressional bending stresses become less negative) as the load grows linearly to 150 MPa at 10 Myr. Plasticity (i.e. frictional slip) starts in the LAD slip zone by ∼7 Myr (Fig. 4a) and creep starts at the base of this zone a few Myr earlier (Fig. 4b). At late times in the load growth period (but before the dead loading period begins) there is simultaneous creep and plasticity at the base of the LAD slip zone (which is discussed in the next section).

When the load stops growing at 10 Myr and becomes a dead load at 150 MPa, creep dominates the deformation at the deepest portion of the zone (Fig. 4b) and the stress distribution starts to relax back towards its lithostatic state (Fig. 3); the differential stresses at these higher temperatures will no longer support further plastic straining because of stress relaxation via creep. Fig. 4(a) shows that after *LT*, the plastic strain contours flatten and become horizontal deep in this zone while the contours higher up (where creep is absent) continue to (slowly) expand. The creep strains in Fig. 4(b) continuously increase after *LT*; the contours expand after *LT* in the high temperature, lower portion of the zone. Therefore, in the higher temperature, deepest areas of the LAD slip zone there is simultaneous faulting and creep during the late load growth period, and after *LT* the faulting stops as creep continues. These are palaeoslip regions, since inspection of the differential stresses (via Mohr's circles) at times after the load growth period shows no indication of there once having been faulting at these locations. That is, plots of Mohr's circles at these late times in palaeoslip zones show small circles that are not close to the failure envelope, thus indicating the cessation of faulting. The indications that faulting had occurred in the past (i.e. palaeoslip) come from the irreversible plastic strains that arose during the load growth period (Fig. 2). The shallower, lower temperature areas of this zone show greater differential stresses and continuing plastic strains as expected with active slip.

In the lateral plastic zone (normal faulting near the flexural bulge) the palaeoslip/active slip phenomenon also occurs. At this location the palaeoslip does not directly involve creep, unlike the LAD slip zone. When loading ceases to increase, the frictional slip that is occurring on the far side of the top-lateral zone stops while slip closer to the load continues (though slowly). Fig. 5 shows the plastic strains at several nodes in the lateral slip zone with time. The palaeoslip nodes show that the plastic strain remains constant soon after *LT*, while active slip nodes show continued faulting. Fig. 6 shows where the normal faulting occurs in our models relative to the peripheral or flexural bulge. Most of the normal faulting at the surface occurs between 120 km and 230 km from the loading symmetry axis. The area of active faulting for the entire simulation duration extends from 120 km to 165 km, while the palaeofaulting extends outward towards the flexural bulge. The continual active faulting exists in the region of greatest plate curvature in the lateral slip zone, as it is most prone to plastic failure. The palaeoslip exists where the topography rises more gradually toward the peak height of the bulge. This sensitivity to stress changes via post-loading creep at depth is what causes active faulting to continue near the region of maximum curvature, while faulting ceases nearby at lower plate curvature.

The effects of post-loading creep on continued slippage on faults has been pointed out previously with respect to the aftershocks of the M_w 6.7 Northridge earthquake (Deng *et al.* 1999). In that paper, model stress increases in the vicinity of a fault from creep at depth have some correlation with the observed aftershocks. The stress increases in their elastic/viscoelastic model are not observed in a medium that has a rheology representative of seismic wave-generating unstable slip (see Section 2), but instead they relate stress increases in an elastic medium to the locations and frequency of aftershock observations. While it is certainly true that aftershocks might be expected in regions of stress buildup, our models would provide a more realistic comparison with aftershock data as they predict the spatial and temporal distribution of zones of fault slippage in response to post-loading creep. As discussed above, overcoming

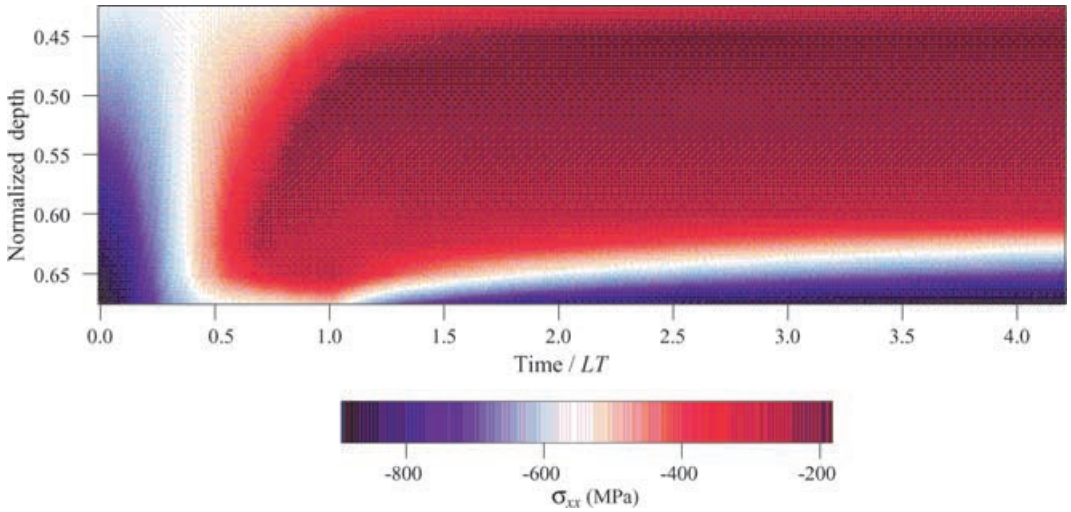

Figure 3. A plot of the total (i.e. deviatoric plus spherical) bending stress (σ_{xx}) in the LAD slip zone as a function of time for the $LT = 10$ Myr simulation. The depth is normalized by the 40 km plate thickness. The plot shows that in the deeper portions of the LAD slip zone, the bending stresses that are accommodated by frictional slip are relaxed via creep for times beyond LT. The shallower, low temperature portion of this zone shows frictional slip starting before $t = LT$ and continuing after $t = LT$.

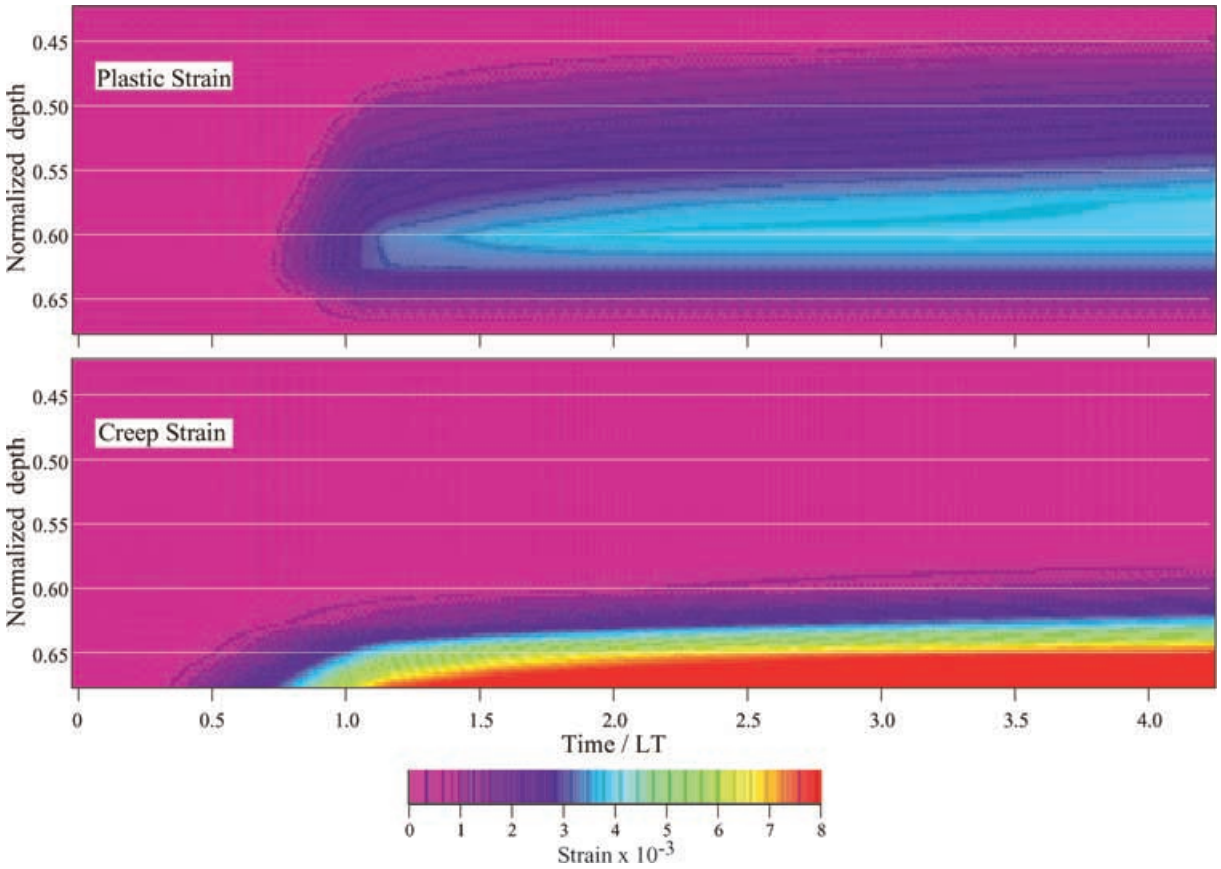

Figure 4. (a) Plastic (frictional slip) strains in the LAD slip zone (with the depth normalized by the plate thickness) along the loading axis for the $LT = 10$ Myr simulation. The horizontality at the lower boundary of the plastic strains indicates that frictional slip is not increasing for times beyond the loadtime. The upper boundary shows expanding contours for plastic strain, showing that frictional slip continues during the same time that the lower plastic strains have ceased. (b) Bending creep strain in the LAD slip zone at the right symmetry (loading) axis continues to increase throughout the entire simulation. The creep strains continue at the expense of frictional slip for depths where the temperature is sufficiently high to cause creep to dominate the inelastic deformation.

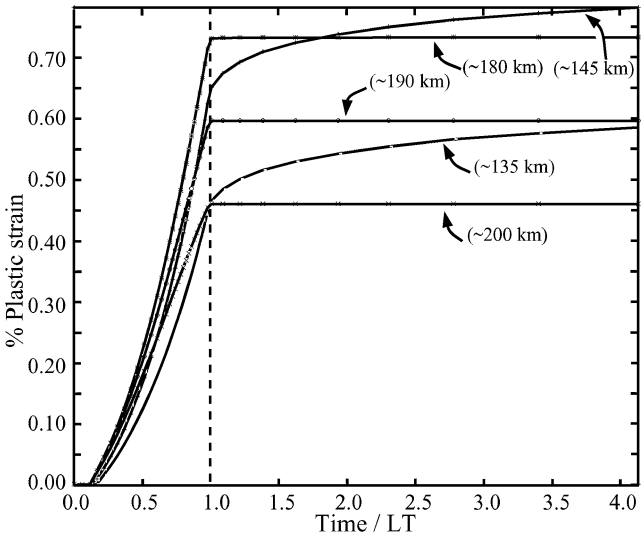

Figure 5. A history plot of several nodes at the surface of the lateral slip zone (normal faulting near the flexural bulge) showing active slip (at ∼135 and 145 km) and palaeoslip (at ∼180, 190 and 200 km). The component of plastic strain that is plotted is in the x-direction (the 'xx' or bending component). The palaeoslip nodes show the same level contours that appear in Fig. 4(a). The active slip nodes show that the plastic strains continue to increase with time, analogous to the expanding contours at the upper boundary in Fig. 4(a). Comparison with Fig. 6 shows that, in general, the active slip occurs toward the direction of the load while palaeoslip occurs outboard of the load. The data is from the $LT = 10$ Myr simulation.

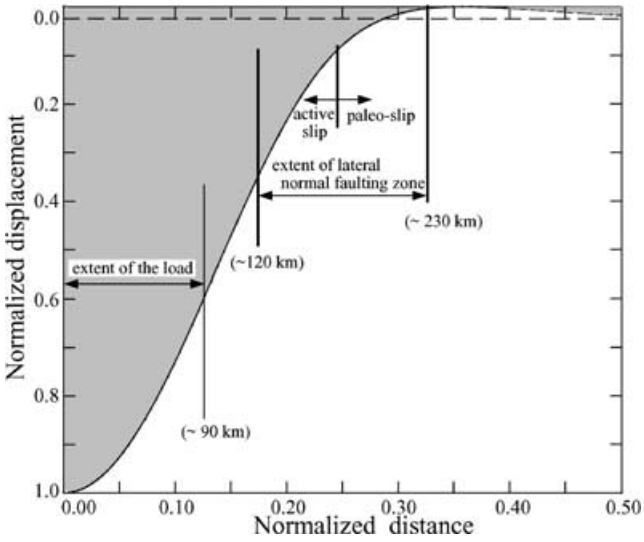

Figure 6. The extent of the lateral slip zone as shown against the displacement along the top surface (where the abscissa is normalized by the 700 km plate length and the ordinate by the maximum surface displacement of ∼6 km). The curve corresponds to the $LT = 1$ Myr model at a time of about 42 Myr. Active faulting occurs toward the direction of the load in the lateral slip zone's region of maximum plate curvature, while palaeofaulting is outboard of this region. The crossover from active slip to palaeoslip occurs at about 165 km from the loading axis.

static frictional fault strength (e.g. as described by the Drucker–Prager model for pressure-dependent frictional slip used here) can be thought of as a necessary (though not sufficient) condition for unstable slip and seismicity. Thus the plastic zones in our model may provide a more precise determination of where aftershocks might take place and how aftershock locations might migrate over time as regions of palaeoslip develop.

Interestingly, in another set of models (Albert & Phillips 2000) that have similar loading but with a cooling 1-D temperature distribution, we find that active slip stops after the onset of dead loading, i.e. the entirety of both normal faulting zones have ceased further slippage and that lithospheric cooling (according to a half-space model, Parsons & Sclater 1977; Turcotte & Schubert 1982) shuts down the post-loading creep and prevents active slip well into the dead loading period, unlike the non-cooling models presented here. Also in that study, we included a thermal perturbation along the plate's loading symmetry axis, which was meant to simulate the effects of a magma conduit. For our chosen 2-D temperature field, both cooling and non-cooling conduit models were devoid of a LAD slip zone, as the high temperatures along the loading symmetry axis prevented stress states that allowed rate-independent plasticity, except at shallow depths where thrust faulting was present. Those results were not discussed in Albert & Phillips (2000), but were deferred to this paper.

4.3 Simultaneous frictional slip and creep

Within the LAD slip zone the models show a narrow band over which frictional slip and creep deformation occur simultaneously during the later stages of the load growth period (Fig. 4). That is, brittle failure via frictional slip and macroscopically continuous deformation via dislocation creep do not have separate regimes over which they operate, but instead conditions favor both mechanisms at the same time in this narrow zone. This narrow band is located at the bottom 3 km of the LAD slip zone (for $LT = 10$ Myr) and coincides with the LAD palaeoslip zone discussed above. This is in contrast to the traditional YSE formulation, where only one inelastic deformation mechanism is permitted at any given depth at a given time. Note that other EVP studies have encountered simultaneous rate-dependent and rate-independent inelasticity under purely compressional external loading (e.g. Gerbault *et al.* 1999; Cloetingh *et al.* 1999). Although our EVP models allow this multiple-mechanism deformation to occur, they do not assure that such deformation is physically realizable for the lithosphere under a particular set of operative $P - T - \dot{\varepsilon}$ conditions:

It is commonly accepted that frictional slip on fracture surfaces gives way to shear rupture of intact rock (as confining pressure increases) where the yield functions of these two pressure-sensitive deformation mechanisms intersect (Byerlee 1968; Paterson 1978). This point of intersection is sometimes referred to as the brittle-ductile transition (BDT) (Kohlstedt *et al.* 1995) and demarcates the transition from macroscopically localized frictional sliding to a macroscopically continuous (ductile) semi-brittle flow. The nature of semi-brittle flow is one of extensive stabilized microcracking plus fine-scale crushing, and limited crystal-plasticity (Paterson 1978; Tullis & Yund 1987; Kachanov 1982; Rutter 1993), so that two fundamentally different deformation mechanisms are present on the same scale and at the same time. One of the roles of crystal-plasticity in this transition zone is crack-tip blunting, which prevents microcrack tips from coalescing into macro-fractures (Courtney 1990; Evans *et al.* 1990) and thus contributes to the stability and relatively uniform distribution of microfracturing. As temperature and confining pressure increase and the brittle-plastic transition (BPT) is encountered, there is a change in the mechanism from semi-brittle flow to fully crystal-plastic flow via dislocation slip, twinning, etc. (Rutter 1986; Evans *et al.* 1990; Kohlstedt *et al.* 1995). Clearly, the

mechanics of semi-brittle flow in the transitional zone between the BDT and BPT are quite complex, and one might expect that a zone of purely cataclastic processes (which deforms in a macroscopically ductile manner) exists below the BDT (as a zone of cataclastic flow), which grades to the combined cataclastic/crystal-plastic deformation of semi-brittle flow down to the BPT. Such deformation has been seen in laboratory work on some rock types and is discussed in Tullis & Yund (1992). The distinction between cataclastic flow (as we use it here, but appears not be universally agreed upon) and semi-brittle flow will need to be further clarified by experimentalists, and has implications for more realistic numerical modelling, as we discuss in Section 5.

Our models do not treat individual fractures *per se* but instead simulate frictional slip in accordance with the traditional method of using a continuum treatment to establish the YSE. So, deep in the LAD slip zone, at the variation from frictional slip to creep in our models, it is more likely that at this depth the variation would be of semi-brittle flow to fully crystal-plastic flow (a microscopically discontinuous, macroscopically continuous deformation to a micro- and macroscopically continuous deformation). We believe, however, that the simultaneous frictional slip and creep behaviour observed in our models is a reasonable first-order step toward modelling the semi-brittle deformation component at the scale of the lithosphere because it shows a pressure-sensitive mechanism operating in conjunction with a pressure-insensitive mechanism. We likely underestimate the amount of pressure-sensitive deformation in this transition region because the frictional strength exceeds the fracture strength of rock at depth beyond the BDT.

As noted above, the narrow 'semibrittle' zone in our model is also a zone of palaeoslip. Thus the dual nature of the deformation ceases just beyond the end of load growth as creep alone relieves stresses in the absence of strain energy input. If viscous stress relaxation is also found at a properly modeled BPT (with a semi-brittle flow-creep transition) as it is with our frictional slip to creep variation, then it suggests that a zone of complex rheology might become simplified when the load has stopped growing. This seems to be a numerical example related to a statement by Rutter (1986) that discusses how intracrystalline plasticity can relax the buildup of tectonic stresses that might otherwise cause seismogenic cataclastic rupture.

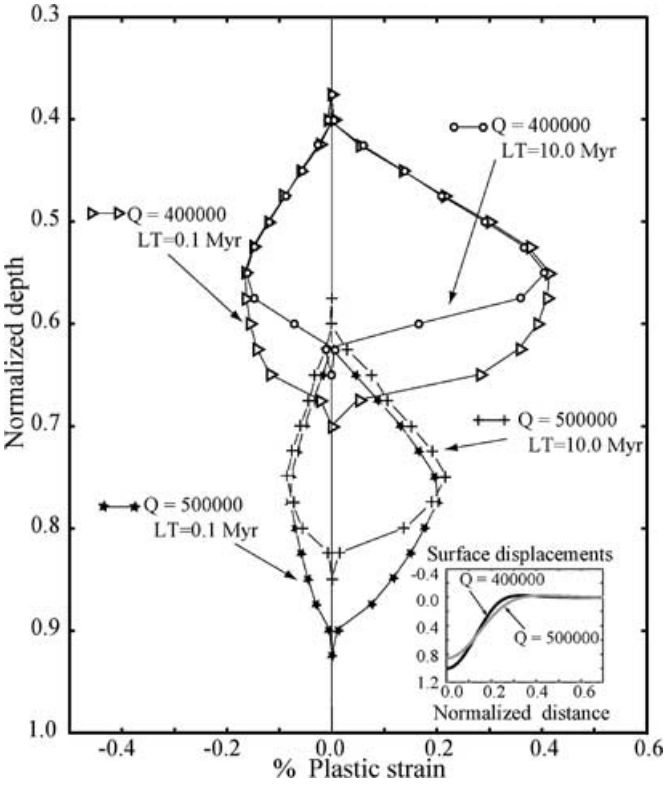

Figure 7. A comparison of the extent of the LAD slip zone (with depth normalized by the plate thickness) for 2 different activation energies (Q) and LTs, shows that an increase of Q causes the zone to be shifted deeper into the plate. The inset figure of surface displacements (normalized by the maximum surface displacement of 6.2 km for the $Q = 400\,000$ J mol^{-1} case) shows the expected weakening of the plate for lower Q. The inset's abcissa is the distance from the loading symmetry axis normalized by the plate length. Both the primary figure and the inset pertain to the final times in the simulations (about 32 Myr after LT), and the curves in the inset are only for $LT = 0.1$ Myr.

4.4 Variation of activation energy for dislocation creep

We also explored the effect of a variation in creep law activation energy (Q) on the depth and extent of the LAD zone (Fig. 7), as it would show the most pronounced effect with a realistic variation relative to other pertinent parameters. We chose Q values of 400 000 J mol^{-1} and 500 000 J mol^{-1}, to cover a realistic range of dislocation creep in weaker and stronger olivine (e.g. Q values of approximately 540 000 J mol^{-1} for dry olivine and dry dunite have been reported in Kohlstedt *et al.* (1995); Mackwell *et al.* (1990); Carter & Tsenn (1987); Karato *et al.* (1986)), and subjected the plates to loading with LT values of 0.1 Myr and 10.0 Myr.

The effect of reduced LT for both Q values is similar to that of our primary wet olivine model (Fig. 2), such that the LAD zone depth extent is increased due to a reduced time for viscous stress relaxation to inhibit rate-independent plasticity. An increase in Q, however, shifts the LAD zone deeper into the plate, as should be expected due to the inhibition of viscous relaxation. In this way the viscous aspect of the plate is compromised, and the elastic-plastic aspect is increasingly favored so that brittle deformation mechanisms can occur at relatively higher temperatures and greater depths compared to the situation where Q is lower. In plates with higher Q, the increased depth to the top of the LAD zone occurs due to the decreased curvature of the plate, i.e. the stronger plate shows a lesser deflection (see inset of Fig. 7) under identical loading, so that the onset of frictional slip (in a normal faulting sense) occurs at a greater depth.

It is also apparent in the figure that the magnitudes of the brittle strains are enhanced for lower Q. This is again because of a larger bending moment (greater deflection) of the weaker plate. Thus, the weaker plate has both enhanced viscous relaxation and enhanced brittle deformation when comparing the magnitudes of these deformation mechanisms relative to a stronger plate under identical loading.

Comparison of surficial active vs paleaoslip in the lateral normal faulting zone (labelled in Fig. 1) with the two different Q values showed that the amount of active slip in this zone is increased for lower Q, as one would expect. The strain rates that pertain to this slip are also much higher for a lower-Q plate, although the amount of strain and its rate are not significantly affected by varying LT for a given Q. Concerning the surficial spatial extent of the lateral slip zone, we find that a stronger plate causes this zone to be somewhat larger, with a reduced maximum in plastic strain. Conversely, the lateral normal faulting zone in a weaker plate covers a lesser spatial

extent at the surface, but its maximum bending plastic strains long after *LT* are much larger.

A variation of other parameters in the creep law (such as the differential stress exponent or creep coefficient) or the gradient in a 1-D temperature field will lead to qualitatively predictable results, so were avoided in this study. Clearly, the most important aspect of these variations would be to inhibit or favor crystal-plastic processes, which will influence the LAD slip zone location and magnitudes of frictional slip and its rates in both zones of normal faulting. The results of our variations of Q are indicative of the changes that will occur when other parameters are varied, within the bounds of the existing assumptions of this study.

5 DISCUSSION AND CONCLUSIONS

The plasticity in this model is not setup to distinguish between stable or unstable slip because we have not included some of the important factors that inhibit or favor stable slip, such as velocity-weakening (Scholz 1990, 1998) or dilatancy-hardening (Rudnicki & Chen 1988). Seismogenesis is related to frictional stability rather than simply fault strength; the base friction coefficient in Byerlee's rule has no implications for the stability of frictional slip (Rutter 1993; Scholz 1998), but does provide a base level which generally must at least be met for seismicity (see Section 2). In spite of the absence of stable or unstable slip distinctions, the implications for the palaeoslip versus active slip phenomena are that fault motions and therefore the potential for earthquakes arise in part by the continued movements via creep within the plate even after a load stops growing. This mechanism has previously been postulated for the genesis of aftershocks (Thatcher & Rundle 1984; Deng *et al.* 1999). The models we presented in this paper implemented a more realistic rheology than these studies, and verified slip and potential seismicity occurring at the top and in the interior of the plate due to continued creep-activated vertical deflection well after dead loading begins at *LT*. Adjustments in the load from mass wasting or erosion (and further load increases, of course) may also contribute to the long-term lithospheric response via creep and perhaps become manifested seismically in the plate.

We believe that the series representation of EVP rheology has some important merits relative to the YSE/EP formulation, as well as viscoelastic (VE) models (Courtney & Beaumont 1983; Watts & Zhong 2000) of the lithosphere. Our results show that the deformation in part of the plate is strongly related to *LT*, as shown in the dependence of the LAD slip zone's spatial extent on the load growth period. This creep-induced time-dependence of plastic failure, absent from YSE/EP and VE formulations, is based on interactions between stress buildup during loading, stress relaxation via time-dependent creep, and time-independent frictional slip. The YSE's abrupt transition from frictional slip (or fracture, if included) to creep precludes the possibility of simultaneous pressure-sensitive and pressure-insensitive mechanisms.

Unfortunately the simultaneity we find in our models does not allow a true reproduction of brittle to ductile cataclastic processes (the latter manifested either as purely cataclastic flow versus semi-brittle flow, according to the distinction we use in Section 4.3) at the BDT nor the semi-brittle flow to fully crystal-plastic transitions (BPT) as observed via experimentation (Paterson 1978; Tullis & Yund 1987). This is because the constitutive relations that are commonly utilized for friction and fracture are generally based on clearly distinguished examples of these mechanisms. The behaviour within the semi-brittle regime lacks established, detailed constitutive information to incorporate into finite element models (Kohlstedt *et al*. 1995). We suggest that a more complex, 4 component series model with a spring, dashpot, sliding block for frictional slip, and sliding block for semi-brittle flow will provide more insight into actual lithospheric behaviour. In addition, the presence or absence of a reasonably distinct zone of cataclastic flow (of purely brittle deformation mechanisms, presumably between the BDT and the onset of semi-brittle flow) would complicate matters further. To the degree that such behaviours can be represented via constitutive equations, a 5 component model (as above but with separate cataclastic flow and semi-brittle flow components between the BDT and BPT) might provide a more realistic numerical model for the lithosphere. However, the transitional component(s) of the model (i.e. between the BDT and BPT) would only give a numerically gross approximation to the complexities observed in experimental work due to the inherent difficulty of constitutively describing such processes. But the results should more closely represent actual brittle-ductile and brittle-plastic transition behaviours relative to a model that allows only a transition from frictional sliding to creep. In addition, models similar to those presented here but pertinent to unstable slip would be instructive regarding how post-loading creep relates to the generation of earthquakes.

Finally, we note that a parabolic or other nonlinear yield surface will better represent, than the Drucker–Prager failure model used here, the nonlinear relationship that is found with fracture as normal stress increases (Paterson 1978; Shimada & Cho 1990; Hoek & Brown 1980; Schultz & Zuber 1994). Some of these functions will also reduce the dilatancy as depth increases, if the computationally favorable associated flow rule is used, resulting in a better representation of rock under increasing pressure.

ACKNOWLEDGMENTS

This work was supported by the Planetary Geology and Geophysics Program under NASA grant NAG5-4448. The authors would like to thank Bob Courtney and an anonymous reviewer for comments that helped to improve the clarity of this paper. In addition, Dan Nunes and Andrew Dombard provided assistance with the latest version of MARC.

REFERENCES

Albert, R.A. & Phillips, R.J., 2000. Paleoflexure, *Geophys. Res. Lett.,* **27,** 2385–2388.

Albert, R.A. & Rudnicki, J.W., 2001. Finite element simulations of Tennessee marble under plane strain laboratory testing: Effects of sample-platen friction on shear band onset, *Mec. Mat.,* **33,** 47–60.

Albert, R.A., Phillips, R.J., Dombard, A.J. & Brown, C.D., 2000. A test of the validity of yield strength envelopes with an elastoviscoplastic finite element model, *Geophys. J. Int.,* **140,** 399–409.

Bassi, G., 1991. Factors controlling the style of continental rifting: Insights from numerical modelling, *Earth planet. Sci. Lett.,* **105,** 430–452.

Bassi, G.C., Keen, C.E. & Potter, P., 1993. Contrasting styles of rifting: Models and examples from the eastern Canadian margin, *Tectonics,* **12,** 639–655.

Bathe, K.-J., 1996. *Finite Element Procedures,* Prentice Hall, Engelwood Cliffs, NJ.

Batt, G.E. & Braun, J., 1997. On the thermomechanical evolution of compressional orogens, *Geophys. J. Int.,* **128,** 364–382.

Bažant, Z.P., 1988. Softening Instability: Part I—Localization Into a Planar Band, *J. appl. Mech.,* **55,** 517–522.

Beaumont, C., Kamp, P.J.J., Hamilton, J. & Fullsack, P., 1996. The continental

collision zone, South Island, New Zealand: Comparison of geodynamical models and observations, *J. geophys. Res.,* **101,** 3333–3359.

Bodine, J.H., Steckler, M.S. & Watts, A.B., 1981. Observations of flexure and the rheology of the oceanic lithosphere, *J. geophys. Res.,* **86,** 3695–3707.

Brace, W.F. & Kohlstedt, D.L., 1980. Limits on lithospheric stress imposed by laboratory experiments, *J. geophys. Res.,* **85,** 6248–6252.

Braun, J. & Beaumont, C., 1987. Styles of continental rifting: Results from dynamic models of lithospheric extension, in, *Sedimentary Basins and Basin-Forming Mechanisms,* Vol. 12, pp. 241–258, eds Beaumont, C. & Tankard, A.J., Canadian Society of Petroleum Geologists Memoir.

Braun, J. & Beaumont, C., 1989. Contrasting styles of lithospheric extension: Implications for differences between Basin and Range province and rifted continental margins, in *Extensional Tectonics and Stratigraphy of the North Atlantic Margins*, Vol. 46, pp. 53–79, eds Tankard, A.J. & Balkwill, H.R., American Association of Petroleum Geologists Memoir.

Brown, C.D. & Grimm, R.E., 1996. Lithospheric rheology and flexure at Artemis Chasma, Venus, *J. geophys. Res.,* **101,** 12 697–12 708.

Burg, J.-P., 1999. Ductile structures and instabilities: their implication for Variscan tectonics in the Ardennes, *Tectonophysics,* **309,** 1–25.

Burov, E.B. & Diament, M., 1995. The effective elastic thickness (T_e) of continental lithosphere: What does it really mean?, *J. geophys. Res.,* **100,** 3905–3927.

Burov, E.B. & Diament, M., 1996. Isostacy, equivalent elastic thickness, and inelastic rheology of continents and oceans, *Geology,* **24,** 419–422.

Byerlee, J.D., 1968. Brittle-ductile transition in rocks, *J. geophys. Res.,* **73,** 4741–4750.

Byerlee, J.D., 1978. Friction of rocks, *Pure appl. Geophys.,* **116,** 615–626.

Carter, N.L., 1976. Steady state flow of rocks, *Rev. Geophys. Space Phys.,* **14,** 301–360.

Carter, N.L. & Tsenn, M.C., 1987. Flow properties of continental lithosphere, *Tectonophysics,* **136,** 27–63.

Chéry, J., Lucazeau, F., Daigniéres, M. & Vilotte, J.P., 1992. Large uplift of rift flanks: A genetic link with lithospheric rigidity?, *Earth planet. Sci. Lett.,* **112,** 195–211.

Cloetingh, S. & Burov, E.B., 1996. Thermomechanical structure of European continental lithosphere: constraints from rheological profiles and EET estimates, *Geophys. J. Int.,* **124,** 695–723.

Cloetingh, S., Burov, E.B. & Poliakov, A., 1999. Lithosphere folding: Primary response to compression? (from Central Asia to Paris basin), *Tectonics,* **18,** 1064–1083.

Courtney, T.H., 1990. *Mechanical Behavior of Materials,* McGraw Hill, Inc., New York.

Courtney, R.C. & Beaumont, C., 1983. Thermally-activated creep and flexure of the oceanic lithosphere, *Nature,* **305,** 201–204.

Deng, J., Hudnut, K., Gurnis, M. & Hauksson, E., 1999. Stress loading from viscous flow in the lower crust and triggering of aftershocks following the 1994 Northridge, California, earthquake, *Geophys. Res. Lett.,* **26,** 3209–3212.

Dieterich, J., 1979. Modeling of rock friction: 1. Experimental results and constitutive equations, *J. geophys. Res.,* **84,** 2161–2168.

Engelder, T., 1993. *Stress Regimes in the Lithosphere,* Princeton University Press, Princeton, New Jersey.

Evans, B., Fredrich, J.T. & Wong, T.-F., 1990. *The Brittle-Ductile Transition in Rocks: Recent Experimental and Theoretical Progress, Geophys. Monogr. Ser.,* Vol. 56, pp. 61–82, eds Duba, A.G., Durham, W.B., Handin, J.W. & Wang, H.F., AGU, Washington, DC.

Gerbault, M., Burov, E.B., Poliakov, A.N.B. & Dagniéres, M., 1999. Do faults trigger folding in the lithosphere?, *Geophys. Res. Lett.,* **26,** 271–274.

Goetze, C. & Evans, B., 1979. Stress and temperature in the bending lithosphere as constrained by experimental rock mechanics, *Geophys. J. R. astr. Soc.*, **59,** 463–478.

Hoek, E. & Brown, E.T., 1980. Empirical strength criterion for rock masses, *J. Geotech. Eng. Div. Am. Soc. Civ. Eng.,* **106,** 1013–1035.

Huismans, R.S., Podladchikov, Y.Y. & Cloetingh, S., 2001. Transition from passive to active rifting: Relative importance of asthenospheric doming and passive extension of the lithosphere, *J. geophys. Res.,* **106,** 11 271–11 291.

Kachanov, M.L., 1982. A micro-crack model of rock inelasticity—Part II: Propagation of micro-cracks, *Mec. Mat.,* **1,** 29–41.

Karato, S.-I., Paterson, M.S. & FitzGerald, J.D., 1986. Rheology of synthetic olivine aggregates: Influence of grain size and water, *J. geophys. Res.,* **91,** 8151–8176.

Karner, G.D., Driscoll, N.W. & Weissel, J.K., 1993. Response of the lithosphere to in-plane force variations, *Earth planet. Sci. Lett.,* **114,** 397–416.

Khan, A.S. & Huang, S., 1995. *Continuum Theory of Plasticity,* John Wiley and Sons, New York.

Kirby, S.H., 1983. Rheology of the lithosphere, *Rev. Geophys.,* **21,** 1458–1487.

Kirby, S.H. & Kronenberg, A., 1987. Rheology of the lithosphere: Selected topics, *Rev. Geophys.,* **25,** 1219–1244.

Kohlstedt, D.L., Evans, B. & Mackwell, S.J., 1995. Strength of the lithosphere: Constraints imposed by laboratory experiments, *J. geophys. Res.,* **100,** 17 587–17 602.

Mackwell, S.J., Bai, Q. & Kohlstedt, D.L., 1990. Rheology of olivine and the strength of the lithosphere, *Geophys. Res. Lett.,* **17,** 9–12.

MARC Analysis Research Corporation, 1994. User's Guides, ver. K6.2, Volumes A-F, Palo Alto, CA.

McGovern, P.J. & Solomon, S.C., 1994. Patterns of stresses and earthquakes in and around large volcanoes, *EOS, Trans. Am. geophys. Un.,* **75,** 16 344.

McNutt, M.K. & Menard, H.W., 1982. Constraints on yield strength in the oceanic lithosphere derived from observations of flexure, *Geophys. J. R. astr. Soc.*, **71,** 363–394.

Mueller, S. & Phillips, R.J., 1995. On the reliability of lithospheric constraints derived from models of outer-rise flexure, *Geophys. J. Int.,* **123,** 887–902.

Ord, A., Vardoulakis, I. & Kajewski, R., 1991. Shear band formation in Gosford Sandstone, *Int. J. Rock Mech. Min. Sci. & Geomech. Abstr.,* **28,** 397–409.

Parsons, B. & Sclater, J.G., 1977. An analysis of the variation of ocean floor bathymetry and heat flow with age, *J. geophys. Res.,* **82,** 803–827.

Paterson, M.S., 1978. *Experimental Rock Deformation—the Brittle Field,* Springer-Verlag, New York, NY.

Phillips, R.J., 1990. Convection-driven tectonics on Venus, *J. geophys. Res.,* **95,** 1301–1316.

Poirier, J.-P., 1980. Shear localization and shear instability in materials in the ductile field, *J. Struct. Geol.,* **2,** 135–142.

Poirier, J.-P., 1985. *Creep of Crystals- High Temperature Deformation Processes in Metals, Ceramics, and Minerals,* Cambridge University Press, Cambridge.

Read, H.E. & Hegemier, G.A., 1984. Strain softening of rock, soil, and concrete—a review article, *Mec. Mat.,* **3,** 271–294.

Regenauer-Lieb, K. & Yuen, D.A., 1998. Rapid conversion of elastic energy into plastic shear heating during incipient necking of the lithosphere, *Geophys. Res. Lett.,* **25,** 2737–2740.

Regenauer-Lieb, K., Yuen, D.A. & Branlund, J., 2001. The initiation of subduction: Criticality by addition of water?, *Science,* **294,** 578–580.

Rudnicki, J.W. & Chen, C.-H., 1988. Stabilization of rapid frictional slip on a weakening fault by dilatant hardening, *J. geophys. Res.,* **93,** 4745–4757.

Rudnicki, J.W. & Rice, J.R., 1975. Conditions for the localization of deformation in pressure-sensitive dilatant materials, *J. Mech. Phys. Solids.,* **23,** 371–394.

Ruina, A., 1983. Slip instability and state variable friction laws, *J. geophys. Res.,* **88,** 10 358–10 370.

Rutter, E.H., 1986. On the nomenclature of mode of failure transitions in rocks, *Tectonophysics,* **122,** 381–387.

Rutter, E.H., 1993. The mechanics of natural rock deformation, in *Comprehensive Rock Engineering*, Vol. 1, Chap. 3, pp. 63–92, ed. Hudson, J.A., Pergamon Press, Oxford.

Shimada, M. & Cho, A., 1990. Two types of brittle fracture of silicate rocks uder confining pressure and their implications in the Earth's crust, *Tectonophysics,* **175,** 221–235.

Scholz, C.H., 1990. *The Mechanics of Earthquakes and Faulting,* Cambridge University Press, Cambridge.

Scholz, C.H., 1998. Earthquakes and friction laws, *Nature,* **391,** 37–42.

Schultz, R.A. & Zuber, M.T., 1994. Observations, models, and mechanisms of failure of surface rocks surrounding planetary surface loads, *J. geophys. Res.,* **99,** 14 961–14 702.

Solomon, S.C. & Head, J.W., 1990. Heterogeneities in the thickness of the elastic lithosphere of Mars: Constraints on heat flow and internal dynamics, *J. geophys. Res.,* **95,** 11 073–11 083.

Thatcher, W. & Rundle, J.B., 1984. A viscoelastic coupling model for the cyclic deformation due to periodically repeated earthquakes at subduction zones, *J. geophys. Res.,* **89,** 7631–7640.

Tse, S.T. & Rice, J.R., 1986. Crustal Earthquake Instability in Relation to the Depth Variation of Frictional Slip Properties, *J. geophys. Res.,* **91,** 9452–9472.

Tullis, J. & Yund, R.A., 1987. Transition from cataclastic flow to dislocation creep of feldspar: Mechanisms and microstructures, *Geology,* **15,** 606–609.

Tullis, J. & Yund, R.A., 1992. The brittle-ductile transition in feldspar aggregates: An experimental study, in *Fault Mechanics and Transport Properties of Rocks*, *Internat. Geophys. Ser.,* Vol. 51, pp. 89–118, eds Evans & Wong, Academic Press, NY.

Turcotte, D.L. & Schubert, G., 1982. *Geodynamics: Applications of Continuum Physics to Geological Problems,* John Wiley, Inc., New York, NY.

Watts, A.B. & Zhong, S., 2000. Observations of flexure and the rheology of oceanic lithosphere, *Geophys. J. Int.,* **142,** 855–875.

Watts, A.B., Bodine, J.H. & Steckler, M.S., 1980. Observations of flexure and the state of stress in the oceanic lithosphere, *J. geophys. Res.,* **85,** 6369–6376.

Zienkiewicz, O.C. & Taylor, R.L., 1989. *The Finite Element Method,* Vol. 2, McGraw Hill, London.